

Influence of nozzle enabling strategy on spray deposition of crop protection unmanned aerial system

Wei Gu^{1,2}, Xinyu Xue^{1,2*}, Chen Chen^{1,2}, Qingqing Zhou^{1,2}, Songchao Zhang^{1,2}, Bin Peng³

(1. Nanjing Institute of Agricultural Mechanization, Ministry of Agriculture and Rural Affairs, Nanjing 210014, China;

2. Key Laboratory of Aviation Plant Protection, Ministry of Agriculture and Rural Affairs, Anyang 455000, Henan, China;

3. XAG Co., Ltd, Guangzhou 510663, China)

Abstract: Proper nozzles arrangement is significant to improve spray deposition of crop protection unmanned aerial system (UAS). Besides fuselage structure, the control strategy is another nozzle location changing method when there are multiple sets of nozzles. A four-rotor crop protection UAS equipped with four centrifugal nozzles was used to conduct a field experiment in the rupturing stage of rice. Two sets of nozzles in the front and rear of the fuselage were enabled independently to investigate spray deposition, including spray coverage and droplet density on the sampling cards. Various nozzle rotating speeds and flight speeds were employed in the experiment to study the influence of nozzle location on the deposition. With different nozzle rotating speeds, the droplet spectrum could be controlled. The results show that the average coverage and average cumulative droplet density are negatively correlated with flight speed. Average droplet density is also negatively correlated with the droplet size. Spray deposition of front nozzles is significantly reduced compared with that of the rear nozzles under the same spray parameters, especially when the droplet size is too large or the flight speed is too fast. The reduction is mainly concentrated in the center area of the spray swath. As a result, the average cumulative droplet density of the front nozzles decreases by 25.96% in total. The average droplet density decreases by 18.54% when the droplet size is smaller than 100 μm , decreases by 25.02% when between 100 μm and 200 μm , and decreases by more than half when larger than 200 μm . This research can provide guidance for the installation of UAS nozzles and spray control strategy design.

Keywords: crop protection, unmanned aircraft system, nozzles arrangement, spray coverage, droplet density

DOI: 10.25165/j.ijabe.20211404.5922

Citation: Gu W, Xue X Y, Chen C, Zhou Q Q, Zhang S C, Peng B. Influence of nozzle enabling strategy on spray deposition of crop protection unmanned aerial system. *Int J Agric & Biol Eng*, 2021; 14(4): 53–61.

1 Introduction

In recent years, agricultural aviation has attracted more and more attention and has become an important part of modern agriculture^[1]. China is the world's largest user of crop protection unmanned aerial systems (UASs) which are playing an increasingly prominent role in disease and pest control. Compared with traditional crop protection machinery, UASs have the advantages of high efficiency, low economic cost and strong terrain adaptability, which is suitable for China's crop protection needs^[2].

A field test is the most direct and necessary work in the research and development of crop protection UASs. The former experiments mainly investigated the influence of UAS types, spray parameters, meteorological conditions, crop characteristics and other factors on deposition and drift^[3]. Qiu et al.^[4], Qin et al.^[5] and Xue et al.^[6,7] mainly used the elution calibration method to extract UAS spray deposition quantity to research deposition or drift in the early days. Then image analysis method^[8,9] was

widely used in UAS spray analysis benefiting from the development of image analysis technology. In the past two years, Wen et al.^[10], Lou et al.^[11] and Wang et al.^[12] applied elution calibration and image analysis simultaneously to find out the correlation between spray deposition and control efficacy. In order to test the distribution of UAS spray droplets more comprehensively, Wang et al.^[13] adopted a 3-dimensional spatial collection frame to collect droplets from multiple directions. Elution calibration has advantages in the quantitative study of liquid volume, while image analysis can calculate the droplet size and density better. Most of these studies showed that there was still a large potential for spray quality improvement of UASs compared with some traditional machines such as boom sprayers^[11,12].

Large manned aircraft is widely used in the western countries. Scholars applied wind tunnel tests and computational fluid dynamics (CFD) simulations to research the spray deposition or drift principles within the wind field of manned aircraft such as propeller wake flow^[14] and wing tip vortex^[15]. Similarly, particle image velocimetry (PIV) tests and CFD simulations were used in China to research the downwash airflow^[16-19] and droplet transportation process^[10,20-24] of rotor UASs. Most of these studies showed that the downwash airflow of the UAS rotor was beneficial to deposition, but swirls and bounces of airflow increased the risk of drift. Compared with the field experiments, indoor experiments or simulations had a visible description of the deposit mechanism of droplets.

The installation location of nozzles had been mentioned in droplet transportation research in some of the above studies, because nozzles determined the size, initial location and initial

Received date: 2020-05-25 **Accepted date:** 2021-01-10

Biographies: Wei Gu, Master, research interest: crop protection and mechanical engineering, Email: guwei525@126.com; Chen Chen, Master, research interest: crop protection and mechanical engineering, Email: 3043095@163.com; Qingqing Zhou, Master, research interest: precise pesticide spraying, Email: 912311431@qq.com; Songchao Zhang, Master, research interest: crop protection and mechanical engineering, Email: 51832898@qq.com; Bin Peng, Bachelor, research interest: unmanned aerial system control technology, Email: pengbin@xair.cn.

*Corresponding author: Xinyu Xue, PhD, Professor, research interest: crop protection and mechanical engineering. Nanjing Institute of Agricultural Mechanization, Ministry of Agriculture and Rural Affairs, Nanjing 210014, China. Tel: +86-25-84346243, Email: xuexynj@qq.com.

velocity of droplets. Wen et al.^[10] discussed the influence of the nozzle location on spray drift of unmanned helicopters by CFD simulation, and proposed that the vertical distance between the nozzles and the fuselage had no obvious influence on spray drift, while spray drift increased with increasing horizontal distance in the width direction. Yang et al.^[24] also studied the droplet transportation of unmanned helicopters by CFD simulation and proposed that optimizing the spray system of the unmanned helicopter could improve the uniformity of droplet deposition distribution without changing the structure design, such as installing different types of nozzles or installing nozzles in a reasonable location. Lian^[25] studied the spraying behavior of nozzles at different locations of the six-rotor UAS with the spray distribution testbed indoor, and proposed that the optimal nozzle location was directly under the rotor. However, there was still a lack of field experiments about the influence of nozzle locations on spray deposition of multi-rotor UASs.

Spray deposition of a crop protection UAS can be improved by the proper arrangement of nozzles. Besides the structure, the nozzle enabling strategy is another nozzle location changing method when there are multiple sets of nozzles. Nowadays, besides hydraulic nozzles, centrifugal nozzles are widely used on crop protection UASs^[26]. A UAS equipped with four centrifugal nozzles under its four rotors was employed in the experiment in the paddy field. Nozzles were divided into two sets by the location of the fuselage. In general, only the rear nozzles were enabled to spray. But when a large flow spraying operation was needed, the front and rear nozzles, namely all nozzles, were used simultaneously to increase the flow rate. Therefore, two sets of nozzles were controlled independently to compare impacts of nozzle enabling strategy. Then, spray coverage and droplet density were studied by the image analysis method, and the possible reasons for the deposition differences between enabling nozzles in the front or the rear were discussed so as to help design and optimize the installation or control strategy of UAS nozzles.

2 Materials and methods

2.1 Experimental materials

A four-rotor crop protection UAS P20 (XAG Co., Ltd, Guangzhou, Guangdong, China) was used in the experiment. Main parameters are shown in Table 1. Full-autonomous mode with real-time kinematic (RTK) positioning and navigation was adopted in the operation to ensure high flight accuracy and flight route repeatability.

Table 1 Main parameters of the UAS P20

Main parameters	Specification or value
Size/mm×mm×mm	1150×1150×400
Nozzle type	Centrifugal nozzle
Nozzle distance/mm	1050
Nozzles amount	4
Nozzle flow rate range/mL·min ⁻¹	150-500
Volume median diameter (VMD) range/μm	70-200
Flight height/m	1.5-3.0
Flight speed/m·s ⁻¹	3-7
Spray volume/L·hm ⁻²	5-15
Spray swath/m	2.5-3.0

The rotors of P20 are arranged in “X” shape, and the four centrifugal nozzles are arranged directly under each rotor, as shown in Figure 1.

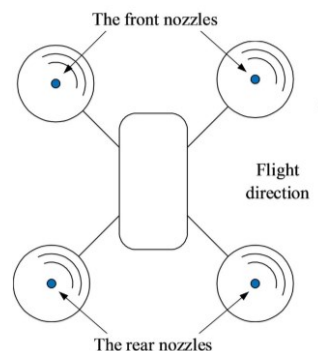


Figure 1 Nozzle location of UAS P20

The meteorology during the experiment was measured by a small weather station Watchdog 2900ET (Spectrum Technologies, Inc., Aurora, IL, USA). As the humidity of the paddy field is extremely high in summer, water-sensitive paper is easy to be invalid affected by moisture and dew. Therefore, the spraying liquid of 5.0 g/L Allura Red aqueous solution, and 76 mm×76 mm blue paper cards (DELI Group Co., Ltd., Ningbo, Zhejiang, China) were used as the sampling cards to collect droplets. After the experiment, sampling cards were scanned by digital scanner 9000F MarkII (Canon Inc., Tokyo, Japan), and the droplets were counted by the software DepositScan (USDA-ARS Application Technology Research Unit, Wooster, OH, USA). The software didn't calibrate the droplet size with ordinary paper^[27], so the absolute size was not accurate, but the comparison of the relative size of droplets was still meaningful. The position and speed of the UAS were monitored in real time by the RTK-based flight route assessment system for crop protection UAS (Nanjing Institute of Agricultural Mechanization, Ministry of Agriculture and Rural Affairs, Nanjing, Jiangsu, China). Static horizontal positioning accuracy of the system is 1.1 cm, and static altitude positioning accuracy is 1.0 cm. When the UAS is flying, horizontal positioning accuracy is 2.5 cm, and altitude positioning accuracy is 2.0 cm.

2.2 Environment and meteorology

The experiment site is located in Wujiang Modern Agriculture Industrial Park of Jiangsu Province (120.7580°E, 31.1825°N). The rice was at the rupturing stage, and the plant height was about 80-90 cm. During the experiment, the average relative humidity was 80.3%, the average temperature was 31.1°C, the average wind speed was 1.72 m/s, and the wind direction was SSE.

2.3 Experiment treatments

In this study, the two nozzles in the front of the flight direction are defined as the front nozzles and the two nozzles in the rear of the flight direction are defined as the rear nozzles. The location definition has no concern with the actual location of the fuselage. The deposition performance was studied by independent spraying with the rear nozzles (R) or the front nozzles (F), respectively. Actually, four nozzles spraying at the same time can be equivalent to the superposition of two independent sprayings.

The centrifugal nozzles were also designed by XAG Co., Ltd. Rotating speed of this type of nozzle can be controlled at 3000-15 000 r/min. With three levels of the rotating speed of 5000 r/min (A), 9000 r/min (B) and 13 000 r/min (C), different droplet size spectra can be obtained.

Flight speed is related to spray volume and nozzle flow rate. The relationship between flight speed and flow rate of one nozzle can be calculated by spraying area Equation (1) and spraying quantity Equation (2) as:

$$svt = 10^4 A \tag{1}$$

$$\frac{nft}{1000 \times 60} = QA \tag{2}$$

where, s is the spraying swath, m; v is the flight speed, m/s; t is the spraying time, s; A is the spraying area, hm^2 ; n is the number of enabled nozzles; f is the single nozzle flow rate, mL/min; Q is the spraying quantity per unit area, L/hm^2 . After combining Equations (1) and (2), Equation (3) can be obtained to present the relationship among these parameters as:

$$Q = \frac{nf}{6sv} \tag{3}$$

Flow rate and flight speed are designed according to the value range in Table 1. Spraying quantity per unit area Q was fixed as $9 \text{ L}/\text{hm}^2$ to ensure the consistency of theoretical deposition quantity per unit area. In the experiment, only a single set of nozzles was enabled to spray, that was, the number of enabled nozzles n was 2. The spraying swath s was set as 3 m to simulate the real working condition. Then Equation (3) is converted into the relationship between nozzle flow rate f and flight speed v as:

$$\frac{f}{v} = 81 \tag{4}$$

According to Equation (4), nozzle flow rate and flight speed were designed as Table 2 to ensure that the spraying quantity per unit area of each test was $9 \text{ L}/\text{hm}^2$.

Table 2 Flow rate of single nozzle and flight speed

No.	Flow rate/ $\text{mL} \cdot \text{min}^{-1}$	Flight speed/ $\text{m} \cdot \text{s}^{-1}$
1	300	3.7
2	400	4.9
3	500	6.2

As long as the proportion of Equation (4) is satisfied, the spraying quantity per unit area remains constant. Herein, the flight speed was set as the researching parameter, and the tests were conducted with different enabled nozzles and nozzle rotating speeds (see Table 3). The tests are numbered from R-A-1 to F-C-3. The treatment numbers such as R-A or A-1 described later in the study represent the test group containing R-A-1, R-A-2 and R-A-3 or R-A-1 and F-A-1.

Table 3 Treatments and parameter combinations

Treatment No.	Enabled nozzles	Flight height/m	Nozzle rotating speed/ $\text{r} \cdot \text{min}^{-1}$	Flight speed/ $\text{m} \cdot \text{s}^{-1}$
R-A-1				3.7
R-A-2	Rear	1.8	5000	4.9
R-A-3				6.2
R-B-1				3.7
R-B-2	Rear	1.8	9000	4.9
R-B-3				6.2
R-C-1				3.7
R-C-2	Rear	1.8	13 000	4.9
R-C-3				6.2
F-A-1				3.7
F-A-2	Front	1.8	5000	4.9
F-A-3				6.2
F-B-1				3.7
F-B-2	Front	1.8	9000	4.9
F-B-3				6.2
F-C-1				3.7
F-C-2	Front	1.8	13 000	4.9
F-C-3				6.2

2.4 Sampling arrangements

The UAS carried out a non-spraying pre-flight with a flight speed of 6.2 m/s first. Flight route, height and speed were recorded through the flight route assessment system. The directions of sampling lines are vertical to the route to ensure the spraying accuracy as shown in Figure 2, so as to reduce the error caused by inaccurate flight.

The origin point in Figure 2 is the starting point, and the trajectory is in the shape of “∩”. The flight height and speed curves are shown in Figure 3. The flight route is divided according to the acceleration and deceleration state, and the length of each section is calculated according to the position of the flight speed boundary point, as listed in Table 4. The cumulative length is the sum of the current section and all previous sections. The three sampling lines are arranged in the center of the constant motion section CD.

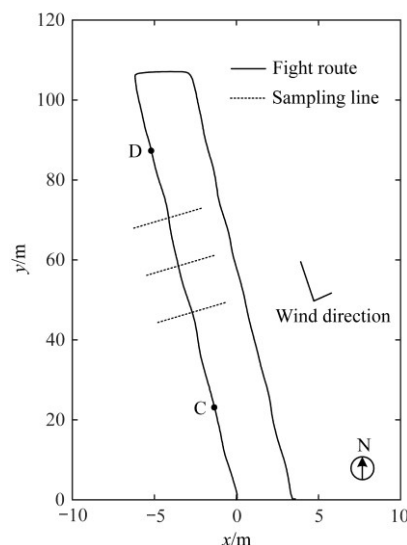


Figure 2 Flight route and sampling line

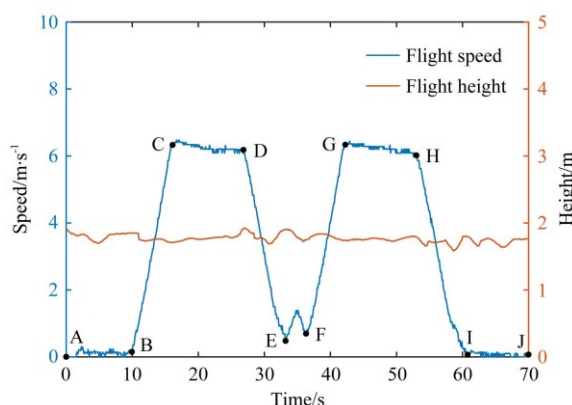


Figure 3 Flight speed and flight height over time

Table 4 Flight route and section length

Section	AB	BC	CD	DE	EF
Status	Hover	Accel	Const	Decel	Trans
Section length/m	0	23.7	65.5	17.4	3.1
Cumulative length/m	0	23.7	89.2	106.6	109.7
Section	FG	GH	HI	IJ	
Status	Accel	Const	Decel	Hover	
Section length/m	19.2	67.3	20.8	0	
Cumulative length/m	128.9	196.2	217.0	217.0	

Note: “Accel” represents accelerated motion, “Const” represents constant motion, “Decel” represents decelerated motion, “Trans” represents transverse motion.

Sampling cards were arranged along the sampling line as shown in Figure 4. Three sampling lines were designed for repeated tests, with a row spacing of 10 m. The real spray swath of UAS is hard to estimate accurately, as it is affected by multiple factors such as spray parameters and the meteorological environment. Therefore, the sampling width of each row was widened to 5 m, wider than the design swath, to capture droplets as many as possible. There were 11 sampling points in each row, with an interval of 0.5 m between each sampling point. Cards were numbered in order, and attached on a shelf 15 cm below the canopy at the sampling points, facing the sky.

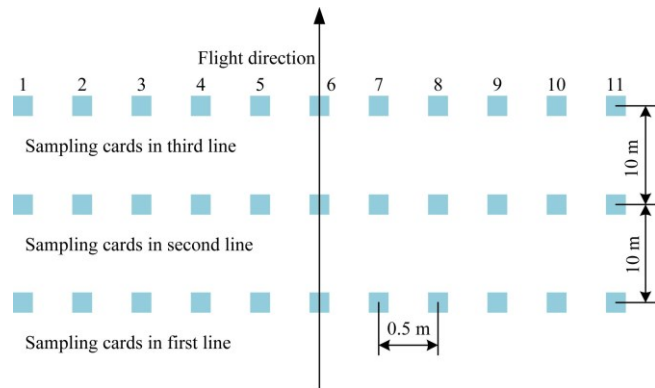


Figure 4 Sampling card arrangements

2.5 Data acquisition and processing

In the tests, the UAS flew autonomously in accordance with the pre-flight route. Nozzle flow rate and rotating speed, flight height and speed were set according to the parameters in Table 3. Nozzles were enabled at point C of the flight route and turned off at point D as shown in Figure 2. Sampling cards were collected after the droplets were dried out, and numbered as (i, j) , where i is the sampling point number from 1 to 11, and j is the line number from 1 to 3.

The collected cards were scanned by the digital scanner and

analyzed by DepositScan to obtain the coverage, droplet density and droplet size. Spray coverage c_p or droplet density d_p of each sampling point is defined as an average value of the same numbered card in three lines.

$$x_i = \frac{\sum_{j=1}^{n_j} x_{(i,j)}}{n_j} \tag{5}$$

where, x_i is the coverage or droplet density of the sampling point i ; $x_{(i,j)}$ is the coverage or droplet density of each sampling card; n_j is the number of lines, which is 3.

Droplet density d_p will be analyzed in various droplet size ranges, and cumulative droplet density d_{cp} is defined as the sum of droplet density d_p in all droplet size ranges on a sampling point.

Average coverage c_a , average droplet density d_a or average cumulative droplet density d_{ca} for one sampling test is defined as an average value of 11 sampling points obtained from Equation (5) given as

$$x_a = \frac{\sum_{i=1}^{n_i} x_i}{n_i} \tag{6}$$

where, x_a is the average value of all sampling points in each test. n_i is the number of sampling points in the single row, which is 11.

3 Results and analysis

3.1 Spray coverage distribution

The spray coverage distribution is shown in Figure 5. c_p in the middle of the sampling line is always obviously larger than that at the two sides, which is consistent with the phenomenon that the spray flow is concentrated under the UAS fuselage. c_p in the middle of the sampling line of the front nozzles is significantly less than that of the rear. When the nozzle rotating speed is 9000 r/min and the flight speed is 3.7 m/s (test group B-1), c_p has the largest decrease of 8.58% of the front nozzles at the sampling location of 0.5 m compared with that of rear nozzles.

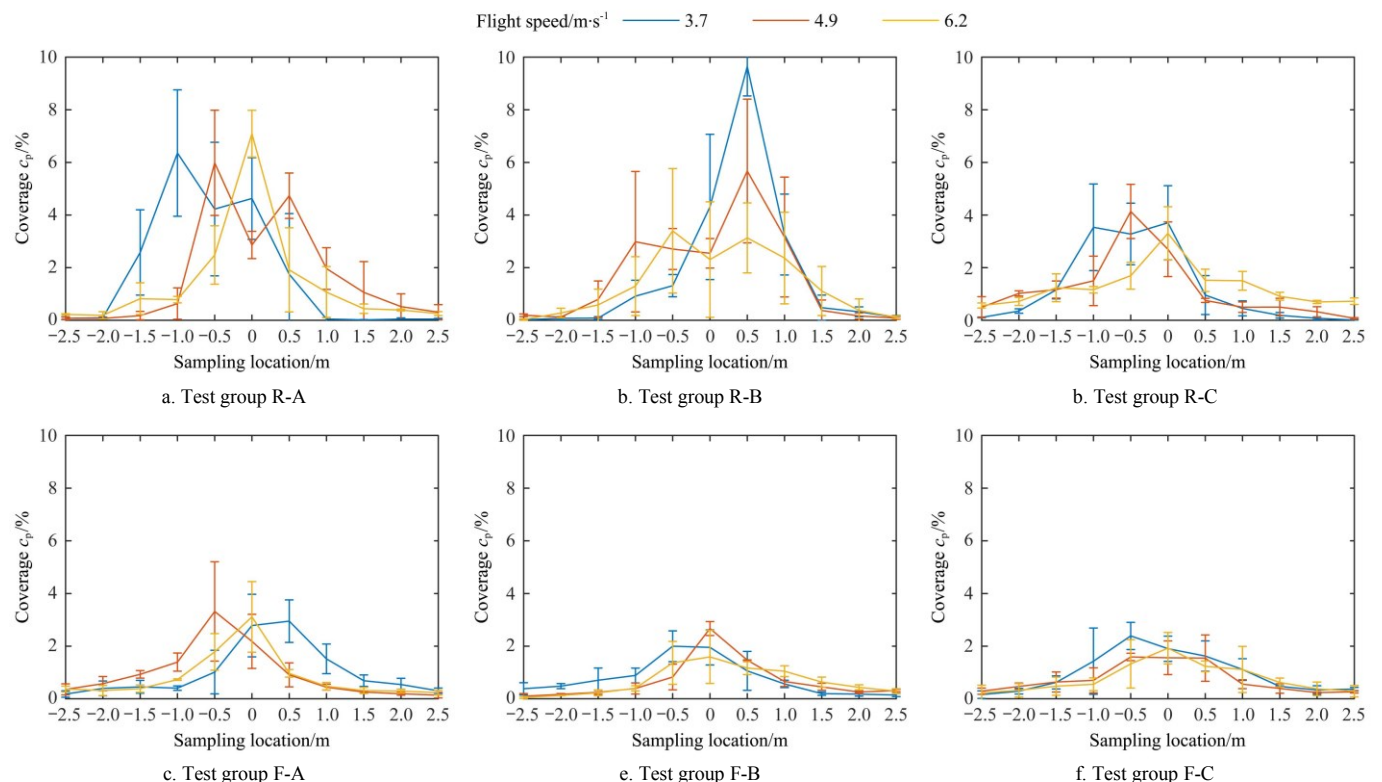


Figure 5 Spray coverage c_p under different treatments

As shown in Figure 5, the influence of nozzle rotating speed and flight speed on coverage distribution is not obvious. c_p of the 11 sampling points in each test was averaged by Equation (6) to obtain c_a . c_a curve is shown in Figure 6 to investigate the relationship between c_a with the flight speed. In general, c_a and flight speed are negatively correlated.

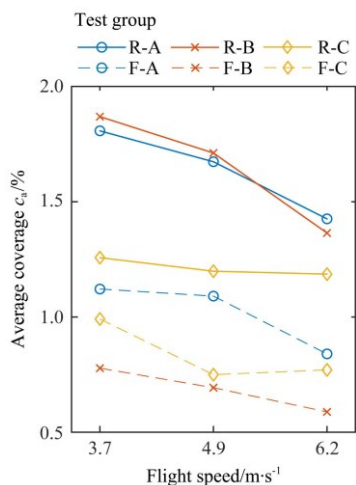


Figure 6 Average coverage c_a of overall points under different treatments

When the rear nozzles are enabled, c_a is almost the same at the nozzle rotating speed of 5000 r/min and 9000 r/min. However, c_a significantly decreases at the rotating speed of 13 000 r/min.

When the front nozzles are enabled, c_a is significantly less than that by enabling the rear nozzles, and it decreases first and then

increases with the rotating speed increasing. In combination with Figure 5, c_p of the front nozzles decreases mostly in the middle, which indicates that a large number of droplets may be lost when enabling the front nozzles, and the loss is mainly concentrated in the center area of the spray swath.

3.2 Droplet density distribution

The droplet density distribution classified by the droplet size ranges is shown in Figures 7 and 8. In general, d_{cp} in the middle of the sampling line is significantly higher than that at the two sides, which is similar to the coverage distribution characters, and d_p in various size ranges also has similar characters. d_p in the middle of the sampling line of the front nozzles is significantly less than that of the rear. When the nozzle rotating speed is 9000 r/min and the flight speed is 3.7 m/s (test group B-1), d_{cp} has the largest decrease of 139.4 droplets/cm² of the front nozzles at the sampling location of 0.5 m compared with that of the rear nozzles.

d_p in various droplet size ranges of the 11 sampling points in each test were averaged by Equation (6) to obtain d_a . d_a with various droplet size ranges are shown in Table 5, where (0,+∞) represents the overall ranges and the values in the column (0,+∞) are d_{ca} . The droplet size can be controlled well by the rotating speed. The number of small droplets increases with the rotating speed, while the large droplet number decreases with the rotating speed. d_a in various droplet size ranges and average cumulative value d_{ca} both decrease with the flight speed in most tests. Meanwhile, d_{ca} curve is shown in Figure 9 to study further. d_{ca} is negatively correlated with the flight speed, but positively correlated with the rotating speed. d_{ca} of the rear nozzles is always more than that of the front under the same treatment.

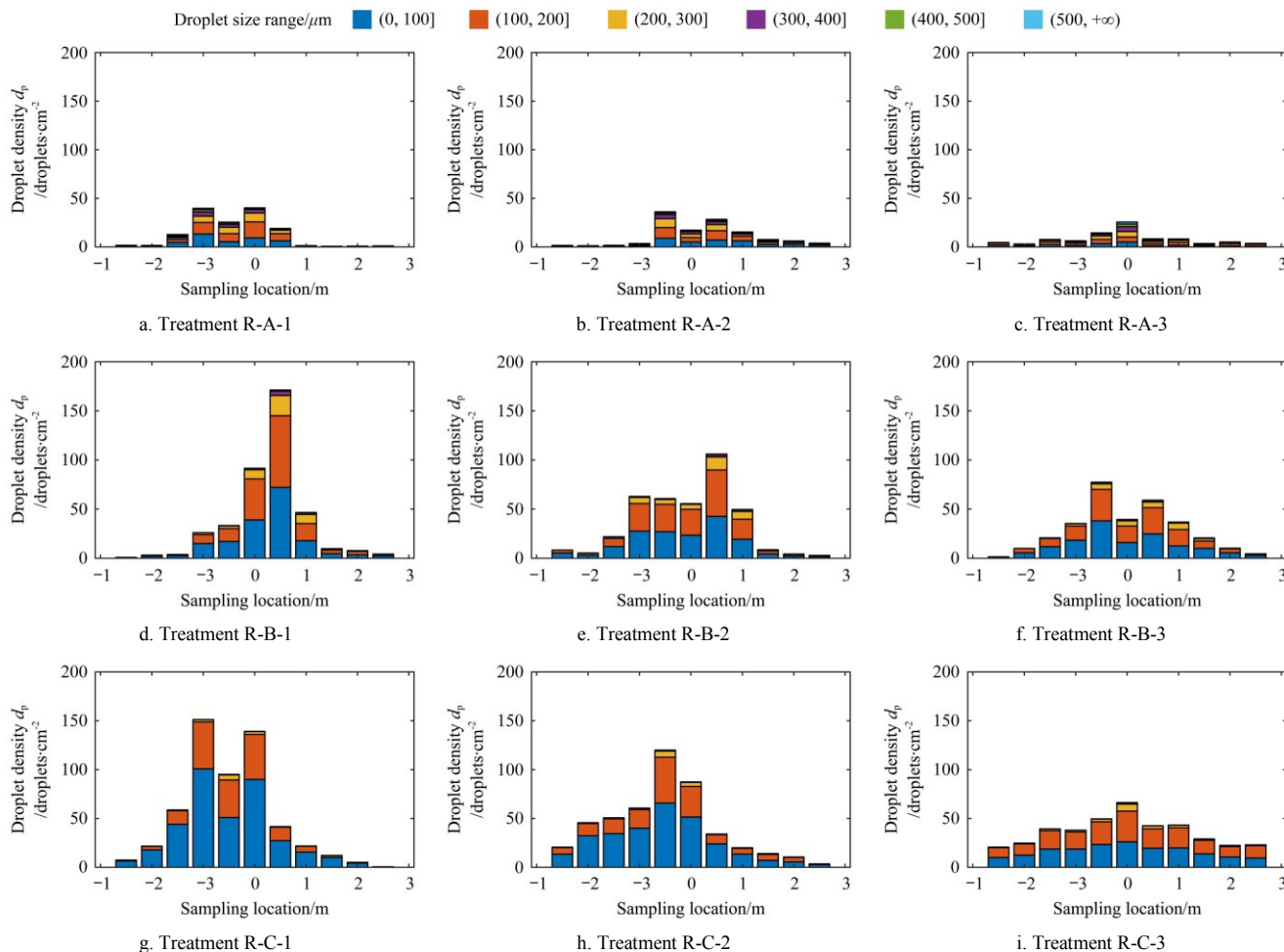


Figure 7 Droplet density d_p in various droplet size range by enabling the rear nozzles

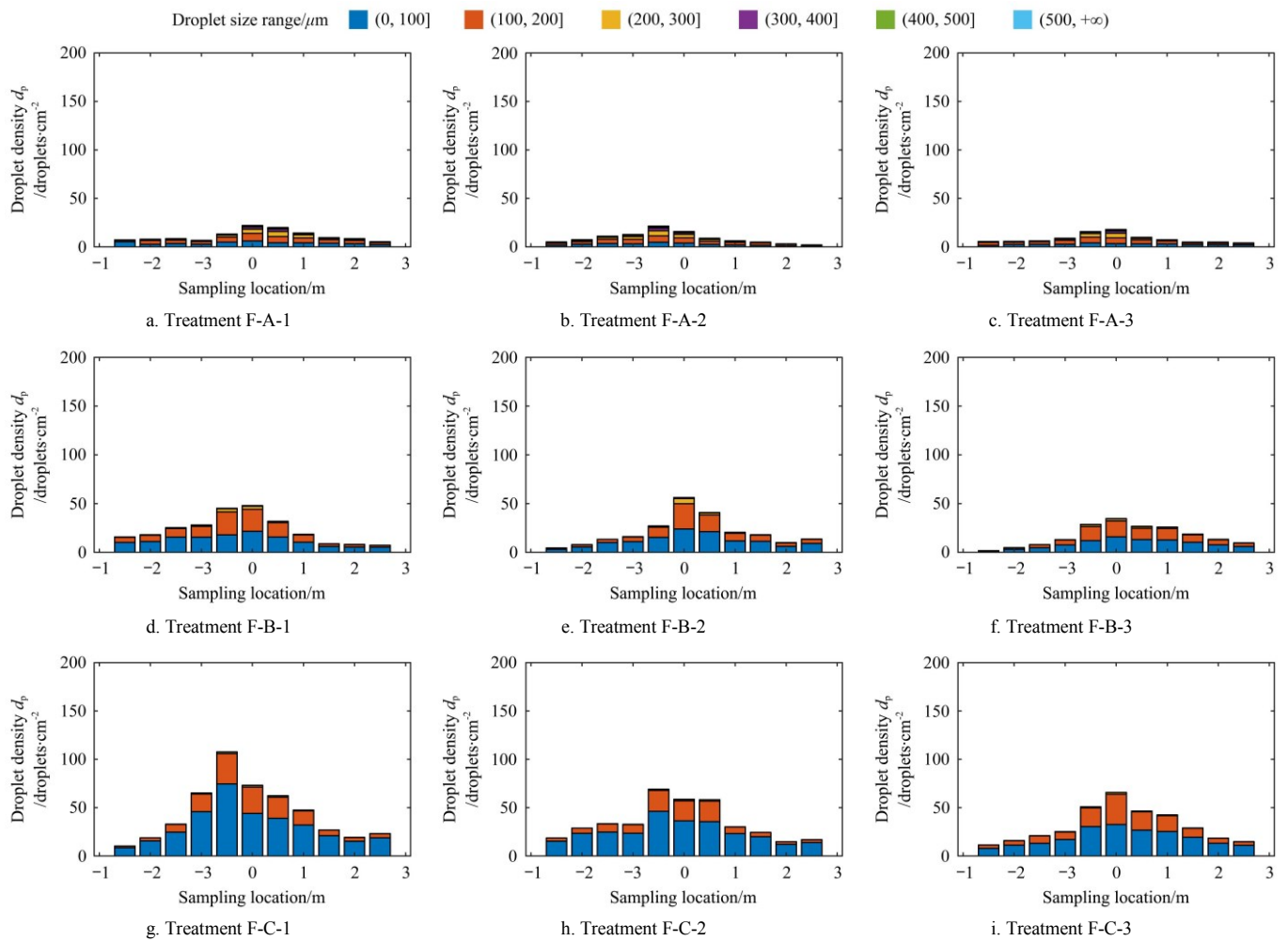


Figure 8 Droplet density d_p in various droplet size range by enabling the front nozzles

Table 5 Average droplet density d_a in various droplet size ranges under different treatments

Treatment No.	Average droplet density d_a /droplets·cm ⁻²						
	(0, 100]	(100, 200]	(200, 300]	(300, 400]	(400, 500]	(500, +∞)	(0, +∞)
R-A-1	3.992	4.496	2.531	1.276	0.591	0.315	13.201
R-A-2	3.505	3.491	2.257	1.177	0.481	0.342	11.254
R-A-3	1.981	2.745	1.797	1.033	0.470	0.298	8.325
R-B-1	16.108	15.080	4.147	0.760	0.119	0.024	36.238
R-B-2	15.312	15.409	3.665	0.612	0.100	0.016	35.115
R-B-3	13.336	12.081	2.677	0.529	0.096	0.019	28.737
R-C-1	33.467	15.812	1.114	0.086	0.011	0.001	50.491
R-C-2	26.443	14.428	1.489	0.154	0.015	0.001	42.530
R-C-3	16.623	17.335	2.126	0.222	0.027	0.002	36.335
F-A-1	3.540	4.234	1.954	0.782	0.269	0.138	10.917
F-A-2	2.466	3.377	1.910	0.797	0.278	0.141	8.969
F-A-3	1.580	2.589	1.476	0.565	0.174	0.085	6.469
F-B-1	12.266	9.737	1.043	0.119	0.020	0.001	23.186
F-B-2	11.710	7.897	1.033	0.125	0.012	0.005	20.781
F-B-3	8.588	7.341	0.828	0.087	0.015	0.002	16.861
F-C-1	30.595	12.551	0.650	0.050	0.008	0.002	43.856
F-C-2	24.938	9.662	0.447	0.027	0.004	0.000	35.077
F-C-3	15.117	11.604	0.527	0.020	0.004	0.001	27.274

As shown in Table 5, when the rear nozzles are enabled, at the rotating speed of 5000 r/min, droplets larger than 300 μm are more than those at the other two rotating speeds under the same flight speed, while the smaller ones are not. Therefore, even though d_{ca}

at the rotating speed of 5000 r/min is significantly less than those at the other two rotating speeds under the same flight speed in Figure 9, c_a is close to that at the rotating speed of 9000 r/min and more than that at the rotating speed of 13 000 r/min as shown in Figure 6.

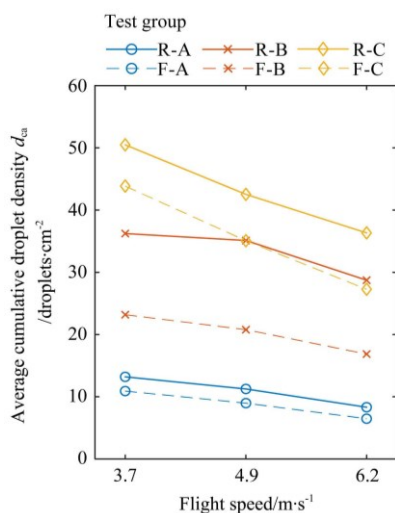


Figure 9 Average cumulative droplet density d_{ca} of overall points under different treatments

When the front nozzles are enabled, droplets larger than $200 \mu\text{m}$ at the rotating speed of 5000 r/min are more than those at the other two rotating speeds, which is quite different from the phenomenon of enabling the rear nozzles.

3.3 Decrease ratio of average droplet density

In order to further investigate the d_a with various droplet size

Table 6 Decrease ratio of average droplet density d_a between enabling rear and front nozzles in various droplet size ranges

Test Group	Decrease ratio of average droplet density $d_a/\%$						
	(0, 100]	(100, 200]	(200, 300]	(300, 400]	(400, 500]	(500, +∞)	(0, +∞)
A-1	11.34	5.82	22.79	38.73	54.39	56.28	17.30
A-2	29.63	3.28	15.39	32.25	42.13	58.93	20.30
A-3	20.28	5.69	17.83	45.36	62.92	71.62	22.30
B-1	23.85	35.43	74.86	84.34	82.82	96.55	36.02
B-2	23.53	48.75	71.80	79.55	88.33	71.16	40.82
B-3	35.60	39.23	69.06	83.60	84.75	89.07	41.33
C-1	8.58	20.62	41.66	41.05	26.52	--	13.14
C-2	5.69	33.03	69.98	82.76	75.00	--	17.52
C-3	9.06	33.06	75.21	90.81	86.14	--	24.94
Mean value	18.54	25.02	51.26	64.64	67.23	73.94	25.96

Note: d_a values in the size range of (500, +∞) in the group C-1, C-2 and C-3 are nearly 0 as shown in Table 5, and they are too small to be calculated for the decrease rate.

4 Discussion

For crop protection UAS, the high spray height and the downwash airflow make the droplet transportation environment more complex than traditional ground machines. In recent years, scholars have used CFD simulations^[10,24] or PIV measure technology^[19,22] to analyze the transportation environment in the UAS spray. They found that the rotor tip vortex would make droplets curl up into a higher space and small droplets much easier to drift, and the high flight speed would enhance this phenomenon^[11]. This can explain the results in this study that the coverage and the droplet density are negatively correlated with the flight speed, but the difference between spray depositions of enabling different nozzles cannot be explained well.

The results from this study show that droplets are lost obviously when enabling the front nozzles. The droplet losses in the center area of spray swath are more serious, and the droplets are lost more easily with increasing droplet size and flight speed. After the UAS spraying, it can be found that some solution is

attached to the surface of devices such as undercarriages or pesticide tank under the fuselage, and such devices are often located in the center area of spray swath. Therefore, it is inferred that the difference between enabling different nozzles results from the number of droplets attached to the undercarriages or pesticide tank.

When sampling cards were identified, the droplets which are obviously larger than others were eliminated. All the sampling cards with extra-large droplets were analyzed again, which were all located at -0.5 m , 0 m or 0.5 m . It indicates that excessive droplets may attach to the central part of the fuselage, which is consistent with the above assumption. A portion of these cards is shown in Figure 10.

In general, crop protection UASs spray in a stable flight, not in hover. Therefore, after leaving from the nozzles, the motion of droplets is not only impacted by the downwash airflow of the rotor, but also by the relative airflow of the environment (commonly known as windward). As shown in Figure 11, a higher flight speed will lead the whole spray flow more backward. If the rear

$$\delta = \frac{d_{ar} - d_{af}}{d_{ar}} \times 100\% \quad (7)$$

where, δ is the decrease ratio, %; d_{ar} is d_a of the rear nozzles, and d_{af} is d_a of the front nozzles at the same nozzle rotating speed and flight speed.

As shown in Table 6, all the decrease ratios are larger than zero. It means that enabling the front nozzles always has larger droplet losses under any same treatment compared with the rear. Mean values of the decrease ratios of 9 groups were calculated in the last row, while decrease ratios of d_{ca} were calculated by Equation (7) in the last column, the mean value of which is 25.96%.

The mean value of decrease ratios increases with the increase of droplet size and the decrease ratio of d_{ca} also increases with the increase of flight speed, that is, the droplets from front nozzles are more difficult to land on the target, especially when droplet size is too large or flight speed is too fast. d_a in the range of (0, 100], (100, 200], (200, 300], (300, 400], (400, 500], and (500, +∞) decreases successively by 18.54%, 25.02%, 51.26%, 64.64%, 67.23%, and 73.94%. Among droplets larger than $200 \mu\text{m}$, more than half of them cannot land on the target.

nozzles are enabled, there will be no obstruction behind the spray flow. While if the front nozzles are enabled, the undercarriages or pesticide tank are behind the spray flow, and the droplet attached increases.

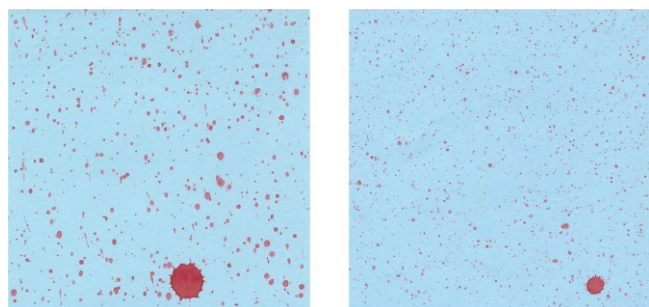


Figure 10 Sampling cards with extra-large droplets

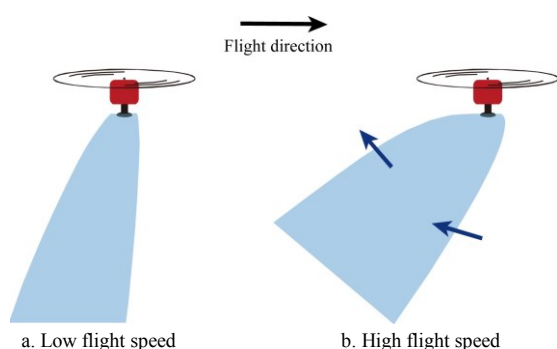


Figure 11 Impact of environment relative airflow on spray flow

In addition, Yang et al.^[18] studied the centrifugal nozzle of a UAS, and proposed that the horizontal deceleration of large droplets was slower than small droplets after leaving from the rotary disks of nozzles, so large droplets were mostly concentrated on the edge of the spray flow, as shown in Figure 12. Therefore, compared with small droplets, large droplets are more likely to hit and attach to the undercarriages or pesticide tank under the fuselage, which means that large droplets are lost more.

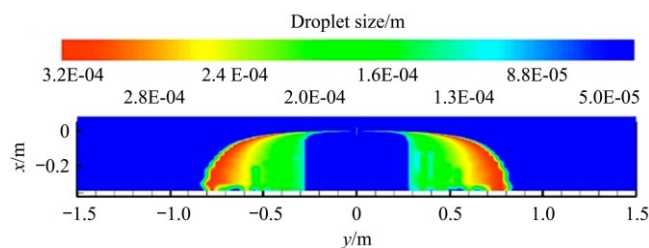


Figure 12 Droplet size distribution at vertical section^[18]

5 Conclusions

Four-rotor crop protection UAS P20 with centrifugal nozzles was employed to study spray coverage and droplet density at the parameters of different nozzle sets in the front or the rear of the fuselage, nozzle rotating speed and flight speed. Through the analysis and discussion of the test results, it can be concluded that:

(1) No matter which nozzle set is enabled, the average coverage and average cumulative droplet density of all tests are negatively correlated with the flight speed, and the average droplet density is also negatively correlated with its size.

(2) Compared with the rear nozzles, the deposit efficiency of droplets with the front nozzles significantly decreases. Increasing the droplet size and flight speed, the average droplet density of the front nozzles decreases even more obviously. The average cumulative droplet density decreases by 25.96%. Moreover, the

average droplet density decreases by 18.54% when the droplet size is smaller than 100 μm , decreases by 25.02% when between 100 μm and 200 μm , and decreases by more than half when larger than 200 μm .

(3) The nozzles should be installed as low as possible and away from other parts of the fuselage, or the nozzles in the front should try not to be enabled during high-speed spraying via control strategy. Due to the large horizontal speed of droplets generated by the centrifugal rotary disk, this problem should be paid more attention to selecting a centrifugal nozzle in a UAS spray system.

Acknowledgements

This research was supported by the National Key Research and Development Program of China (Grant No. 2017YFD0701000), the Science and Technology Development Plan of Suzhou (Grant No. SNG2020042), China Agriculture Research System of MOF and MARA (Grant No. CARS-12) and the Special Expenses for Basic Scientific Research of Chinese Academy of Agricultural Sciences (Grant No. SR201903).

References

- [1] Zhou Z Y, Ming R, Zang Y, He X G, Luo X W, Lan Y B. Development status and countermeasures of agricultural aviation in China. *Transactions of the CSAE*, 2017; 33(20): 1–13. (in Chinese)
- [2] Lan Y B, Chen S D. Current status and trends of plant protection UAV and its spraying technology in China. *Int J Precis Agric Aviat*, 2018; 1(1): 1–9.
- [3] Liao J, Zang Y, Zhou Z Y, Luo X W. Quality evaluation method and optimization of operating parameters in crop aerial spraying technology. *Transactions of the CSAE*, 2015; 31(S2): 38–46. (in Chinese)
- [4] Qiu B J, Wang L W, Cai D L, Wu J H, Ding G Y, Guan X P. Effects of flight altitude and speed of unmanned helicopter on spray deposition uniform. *Transactions of the CSAE*, 2013; 29(24): 25–32. (in Chinese)
- [5] Qin W C, Xue X Y, Zhou L X, Zhang S C, Sun Z, Kong W, et al. Effects of spraying parameters of unmanned aerial vehicle on droplets deposition distribution of maize canopies. *Transactions of the CSAE*, 2014; 30(5): 50–56. (in Chinese)
- [6] Xue X Y, Tu K, Qin W C, Lan Y B, Zhang H H. Drift and deposition of ultra-low altitude and low volume application in paddy field. *Int J Agric & Biol Eng*, 2014; 7(4): 23–28.
- [7] Xue X Y, Lan Y B, Sun Z, Chang C, Hoffmann W C. Develop an unmanned aerial vehicle based automatic aerial spraying system. *Computers & Electronics in Agriculture*, 2016; 128: 58–66.
- [8] Chen S D, Lan Y B, Li J Y, Zhou Z Y, Jin J, Liu A M. Effect of spray parameters of small unmanned helicopter on distribution regularity of droplet deposition in hybrid rice canopy. *Transactions of the CSAE*, 2016; 32(17): 40–46. (in Chinese)
- [9] Qin W C, Qiu B J, Xue X Y, Chen C, Xu Z F, Zhou Q Q. Droplet deposition and control effect of insecticides sprayed with an unmanned aerial vehicle against plant hoppers. *Crop Protection*, 2016; 85: 79–88.
- [10] Wen S, Han J, Lan Y B, Yin X C, Lu Y H. Influence of wing tip vortex on drift of single rotor plant protection unmanned aerial vehicle. *Transactions of the CSAM*, 2018; 49(8): 127–137,160. (in Chinese)
- [11] Lou Z X, Xin F, Han X Q, Lan Y B, Duan T Z, Fu W. Effect of unmanned aerial vehicle flight height on droplet distribution, drift and control of cotton aphids and spider mites. *Agronomy*, 2018; 8(9): 187.
- [12] Wang G B, Lan Y B, Qi H X, Chen P C, Hewitt A J, Han Y X. Field evaluation of an unmanned aerial vehicle (UAV) sprayer: effect of spray volume on deposition and the control of pests and disease in wheat. *Pest management science*, 2019; 75: 1546–1555.
- [13] Wang C L, He X K, Wang X N, Wang Z C, Wang S L, Li L L, et al. Testing method of spatial pesticide spraying deposition quality balance for unmanned aerial vehicle. *Transactions of the CSAE*, 2016; 32(11): 54–61. (in Chinese)
- [14] Thomson S J, Womac A R, Mulrooney J E. Reducing pesticide drift by considering propeller rotation effects from aerial application near buffer zones. *Sustainable Agriculture Research*, 2013; 2(3): 41–51.
- [15] Ryan S D, Gerber A G, Holloway G. A computational study on spray

- dispersal in the wake of an aircraft. *Transactions of the ASABE*, 2013; 56(3): 847–868.
- [16] Zhang S C, Xue X Y, Sun Z, Zhou L X, Jin Y K. Downwash distribution of single-rotor unmanned agricultural helicopter on hovering state. *Int J Agric & Biol Eng*, 2017; 10(5): 14–24.
- [17] Yang F B, Xue X Y, Cai C, Zhou Q Q. Effect of down wash airflow in hover on droplet motion law for multi-rotor unmanned plant protection machine. *Transactions of the ASABE*, 2018; 34(02): 64–73. (in Chinese)
- [18] Guo Q W, Zhu Y Z, Tang Y, Hou C J, He Y, Zhuang J J. CFD simulation and experimental verification of the spatial and temporal distributions of the downwash airflow of a quad-rotor agricultural UAV in hover. *Computers and Electronics in Agriculture*, 2020; 172: 105343. doi: 10.1016/j.compag.2020.105343.
- [19] Tang Q, Zhang R R, Chen L P, Xu G, Deng W, Ding C C, et al. High-accuracy, high-resolution downwash flow field measurements of an unmanned helicopter for precision agriculture. *Computers & Electronics in Agriculture*, 2020; 173: 105390. doi: 10.1016/j.compag.2020.105390.
- [20] Zhang S C, Xue X Y, Qin W C, Sun Z, Ding S M, Zhou L X. Simulation and experimental verification of aerial spraying drift on N-3 unmanned spraying helicopter. *Transactions of the ASABE*, 2015; 31(3): 87–93. (in Chinese)
- [21] Wang J F, Xu W B, Wen J L, Wang X Y, Luo B T. Numerical simulation on gas-liquid phase flow of large-scale plant protection unmanned aerial vehicle spraying. *Transactions of the CSAM*, 2017; 48(9): 62–69. (in Chinese)
- [22] Tang Q, Zhang R R, Chen L P, Xu M, Yi T C, Zhang B. Droplets movement and deposition of an eight-rotor agricultural UAV in downwash flow field. *Int J Agric & Biol Eng*, 2017; 10(3): 47–56.
- [23] Yang F B, Xue X Y, Cai C, Sun Z, Zhou Q Q. Numerical simulation and analysis on spray drift movement of multirotor plant protection unmanned aerial vehicle. *Energies*, 2018; 11(9): 2399. doi: 10.3390/en11092399.
- [24] Yang Z L, Ge L Z, Qi L J, Cheng Y F, Wu Y L. Influence of UAV rotor down-wash airflow on spray width. *Transactions of the CSAM*, 2018; 49(1): 116–122. (in Chinese)
- [25] Lian Q. Study on the variation of downwash and the installation position of nozzles in a six-rotor plant protection drone. PhD dissertation. Daqing: Heilongjiang Bayi Agricultural University, 2019; 6. 109 p.
- [26] Wang G B, Han Y X, Li X, Andaloro J, Chen P C, Hoffmann W C, et al. Field evaluation of spray drift and environmental impact using an agricultural unmanned aerial vehicle (UAV) sprayer. *Science of the Total Environment*, 2020; 737: 139793. doi: 10.1016/j.scitotenv.2020.139793.
- [27] Zhu H P, Salyani M, Fox R. A portable scanning system for evaluation of spray deposit distribution. *Computers & Electronics in Agriculture*, 2011; 76(1): 38–43.